Polymer 49 (2008) 4358–4368

Contents lists available at ScienceDirect

Polymer

journal homepage: www.elsevier.com/locate/polymer

Relation between the viscoelastic and flammability properties of polymer nanocomposites☆

Takashi Kashiwagi [a,*], Minfang Mu [b], Karen Winey [b], Bani Cipriano [c], S.R. Raghavan [c], Seongchan Pack [d], Miriam Rafailovich [d], Yin Yang [e], Eric Grulke [e], John Shields [a], Richard Harris [a], Jack Douglas [f]

[a] Fire Research Division, National Institute of Standards and Technology, Gaithersburg, MD 20899, United States
[b] Department of Chemical and Biomolecular Engineering, University of Pennsylvania, Philadelphia, PA 19104, United States
[c] Department of Chemical and Biomolecular Engineering, University of Maryland, College Park, MD 20742, United States
[d] Materials Science and Engineering Department, Stony Brook University, Stony Brook, NY 11794, United States
[e] Department of Chemical and Materials Engineering, University of Kentucky, Lexington, KY 40506, United States
[f] Polymers Division, National Institute of Standards and Technology, Gaithersburg, MD 20899, United States

ARTICLE INFO

Article history:
Received 12 June 2008
Received in revised form 16 July 2008
Accepted 18 July 2008
Available online 3 August 2008

Keywords:
Nanocomposites
Rheology
Flammability

ABSTRACT

Previous work has shown that the formation of a network structure of nanoparticles within a polymer matrix can significantly reduce nanocomposite flammability and that viscoelastic properties could be utilized to predict their flammability reduction. The present work extends this type of investigation to the study of clay and carbon nanotube nanocomposites. In particular, we study PS/clay, PS/MWNT, PMMA/clay, and PMMA/SWNT nanocomposites. At a clay level of about 10% by mass, the network structure is formed for the PS and the PMMA clay nanocomposites; it requires a level of about 0.5% with the SWNT and 2% with the MWNT. These samples showed significantly reduced mass loss rates of PS and PMMA. However, the solid residues collected from radiative gasification tests of PS/clay and PMMA/clay showed many small cracks, despite the network formation within the initial sample. This is in contrast to the smooth, continuous residues (no cracks or openings) for PS/MWNT and PMMA/SWNT nanocomposites. The cracks in the clay samples are probably formed due to weaker network at elevated temperatures due to weaker bridging interaction between clay platelets as compared to stronger network resulting from dense entanglement and bridging of carbon nanotubes.

Published by Elsevier Ltd.

1. Introduction

The use of nanoparticles in polymeric materials to form polymer nanocomposites has been demonstrated as one of alternative flame retardant approaches to the use of halogenated flame retardants [1–4]. A book reviewing this approach with clay particles, carbon nanotubes, carbon nanofibers, and others was recently published describing flame retardant mechanisms and many applications [5].

We briefly review the physical nature of polymer burning and how the nanoparticles alter this process. The burning process of a polymeric material typically begins with heating to a temperature at which thermal degradation initiates. The boiling temperatures of most of the thermal degradation products of polymers are much lower than the thermal degradation temperatures of thermoplastics, and the degradation products are then superheated and nucleated to form bubbles [6]. These bubbles are formed at and below the heated surface, where thermal degradation occurs, and they grow with the supply of more degradation products by diffusion from the surrounding molten plastic [7]. The bubbles burst at the heated surface evolving their contents into the gas phase as fuel vapor. One flame retardant approach is to suppress the bubbling rate, so as to reduce the supply rate of fuel by forming a protective and heat shielding char layer. A similar approach, that of forming a solid jammed network structure consisting of carbon nanotubes with tangled polymer chains has been demonstrated; this inhibits the otherwise vigorous bubbling process seen in the course of thermal degradation during combustion [8]. This previous study showed a close relationship between viscoelastic characteristics and the flammability properties of thermoplastic-based polymer nanocomposites. In separate work, it has also been reported that the flammability of polymer–clay nanocomposites is reduced with an increase in melt viscosity and the formation of network [9,10].

☆ This is a publication of the National Institute of Standards and Technology (NIST), an agency of the US Government, and by statute is not subject to copyright in the US.

* Corresponding author. Tel.: +1 301 9756699; fax: +1 301 9754052.
E-mail address: takashi.kashiwagi@nist.gov (T. Kashiwagi).

0032-3861/$ – see front matter Published by Elsevier Ltd.
doi:10.1016/j.polymer.2008.07.054

In this study, we examine whether such a relationship can be generalized to polymer nanocomposites based on two different polymer matrices, and clay particles and carbon nanotubes. If such a close relationship between the two properties is demonstrated, the measurement of viscoelastic characteristics could be used as a screening test for flammability before preparing a large quantity of materials. Furthermore, since viscoelastic and flammability properties of polymer nanocomposites depend strongly on the dispersion metrics of nanoparticles in the composites [11–14], such a screening test would be ideal to assure the achievement of intended physical and flammability performance.

2. Experimental section

2.1. Materials

The matrix polymers used in this study were polystyrene, PS (Styron 666D, Dow Chemical, mass-average molecular mass, M_w of 240,000 g/mol with a polydispersity of 2.29) and poly(methyl methacrylate), PMMA (Polysciences, M_w 100,000 g/mol)[1]. Organo-modified montmorillonite clays with dimethyl, dehydrogenated tallow, quaternary ammonium, Cloisite 15A, and with methyl, tallow, bis-2-hydroxyethyl, quaternary ammonium, Cloisite 30B, were kindly provided by Southern Clay Products Inc. and were used as the clay particles. Single-walled carbon nanotubes, SWNTs, were kindly provided by Carbon Nanotechnologies Inc. and Foster Miller Co. Multi-walled carbon nanotubes, MWNTs, were made using xylene as a carbon source and ferrocene as a catalyst at about 675 °C by a chemical vapor deposition, CVD, method at the University of Kentucky [15].

2.2. Composites preparation

The sample preparation of polymer nanocomposites affects their morphology. Therefore, melt blending using a twin-screw extruder for PMMA/Cloisite 30B and PS/MWNT and solvent blending for PMMA/SWNT and PS/Cloisite 15A were used to exclude the effects of sample preparation as much as possible.

PS/Cloisite 15A nanocomposites were prepared by solvent casting method. A dispersion of 1% Cloiste 15A in chloroform was prepared by sonication for 5 min, followed by stirring for 2 h. A solution of 10 mass% PS in chloroform and the Cloisite 15A dispersion were combined, and the mixture was stirred for 24 h. Thereafter, the mixture was cast into an aluminum foil pan and the chloroform evaporated in a hood overnight. The nanocomposite was then further dried and annealed at 160 °C in a vacuum oven for 48 h. PS/MWNT composites were melt blended in a Haake PolyLab shear mixer at the University of Kentucky. The mixture temperature was set at 180 °C and the PS pellets were added to the mixer running at a speed of 20 rpm. The pellets melted in about 3 min, and the MWNTs were then added and mixing was then continued for 40 min.

PMMA/Cloisite 30B nanocomposites were prepared by melt blending in a B & P Process Equipment and Systems twin-screw extruder (co-rotating, intermeshing, L:D equals 25:1) at NIST. Operating conditions were 250 rpm screw speed and 190 °C in all zones with a feed rate of 2 kg/h. The coagulation method was used to produce the PMMA/SWNT nanocomposites [16]. In the coagulation method, dimethyl formamide (DMF) was chosen to dissolve the PMMA and to permit dispersion of the SWNTs by bath sonication for 24 h. Atomic force microscopy (AFM) results show that the average nanotube bundle diameter is about ~7 nm at the concentration of 0.2 mg of SWNT per milliliter of DMF. The content of the SWNT in the nanocomposites varied from 0.2% to 1% by mass.

All samples for measuring flammability properties (discs of 75 mm diameter and 4 mm thickness) were compression molded in the range of 190–210 °C under a pressure of about 1.4 MPa for a duration of 15 min.

2.3. Sample characterization

The morphologies of the nanoparticles in the composite samples were evaluated using a laser confocal microscope (Model LSM510, Carl Zeiss Inc.) to image the nanoparticles in the polymer matrix. The confocal microscope utilizes coherent laser light and collects reflected light exclusively from a single plane with a thickness of 100 nm (a pinhole sits conjugated to the focal plane and rejects light out of the focal plane). A red laser ($\lambda = 633$ nm) was used as the coherent light and images were taken at 100× magnification with an Epiplan-Neofluar 100×/1.30 oil-pool objective. An LP385 (Rapp Opto Electronic) filter was used to limit the lower spectra of reflected light. Two-dimensional images with 512 pixels × 512 pixels were taken with scan size 92.1 × 92.1 μm.

The X-ray diffraction data were collected with Philips XRG 3100 equipped with a Cu Kα radiation ($\lambda = 0.154$ nm) operated at 40 kV and 35 mA with a 0.04° 2θ step size and a 3 s count time per step. Rheology measurements were performed on a Rheometric Solid Analyzer (RSAII) in oscillatory shear with a sandwich fixture. Samples 12.5 mm × 16 mm × 0.5 mm were run at 200 °C with a strain of 0.5% for frequency sweep and at a frequency of 1 rad/s from 160 °C to 240 °C for temperature sweep, all in nitrogen. Thermogravimetric analysis (TGA) was conducted using a TA Instruments TGA Q500 at 5 °C/min from 90 °C to 500 °C in nitrogen (flow rate of 60 cm^3/min) for the original nanocomposite samples (about 5 mg) in a platinum pan.

Scanning electron microscopy, SEM, was conducted with SEM (LEO-1550) with Schottky Field-Emission Gun. A few micrograms of the residues corrected after the radiant gasification test described below were mounted on a specimen holder and then a few micrometers of gold were coated on the surface of the residues in order to make the specimens conductive.

2.4. Flammability property measurement

A radiant gasification apparatus, somewhat similar to a cone calorimeter, was designed and constructed at NIST to study the gasification processes of samples by measuring mass loss rate and temperatures of a sample exposed to a fire-like heat flux in a nitrogen atmosphere (no burning). The apparatus consists of a stainless-steel cylindrical chamber that is 1.70 m tall and 0.61 m in diameter. In order to maintain a negligible background heat flux, the interior walls of the chamber are painted black and the chamber walls are water-cooled to 25 °C. All experiments were conducted at 50 kW/m^2. There are three unique features of this device: (1) observation and results obtained from it are only based on the condensed phase processes due to the absence of any gas phase oxidation reactions and processes; (2) it enables visual observations of gasification behavior of a sample using a video camera under a radiant flux similar to that of a fire without any interference from a flame; (3) the external flux to the sample surface is well-defined and nearly constant over the duration of an entire experiment (and over the spatial extent of the sample surface) due to the absence of heat feedback from a flame. A more detailed discussion of the apparatus is given in a previous study

[1] Certain commercial equipments, instruments, materials, services or companies are identified in this paper in order to specify adequately the experimental procedure. This is no way implies endorsement or recommendation by NIST.

[17]; the standard relative uncertainty of the measured mass loss rate is ±10%.

3. Results

3.1. Sample morphology

The distribution of the nanoparticles in the four different samples was examined by laser confocal microscopy to globally observe the dispersion of the nanoparticles on a micrometer scale. The resulting images are shown in Fig. 1. Fig. 1a indicates that SWNT bundles are relatively uniformly distributed within the PMMA matrix. The average size of SWNT bundles was about 7 nm in diameter and 310 nm in length [18]. The image of PS/MWNT (1% by mass), Fig. 1b, shows entanglement of individual MWNTs throughout the PS matrix and good dispersion of the tubes on a micrometer scale. The average diameter and length of the MWNT in PS were 75 nm and 11.3 μm, respectively [19]. The images of PMMA/Cloisite 30B (10%), Fig. 1c, and PS/Cloisite 15A (10%), (d), show some small aggregates of clay particles but the overall dispersion of the clay particles appears to be reasonably good on this scale. It is important to examine that both PMMA/Cloisite 30B and PS/Cloisite 15A samples are nanocomposites on a nanometer scale and not microcomposites. X-ray diffraction measurements were conducted for these samples and the results are shown in Fig. 2. For PMMA/Cloisite 30B samples, the *d* spacing for the composites, about 32–33 Å, is much larger than that for Cloisite 30B, which is about 18.5 Å. This indicates that PMMA chains are in the galleries and it is considered that the PMMA/Cloisite 30B samples are intercalated. Since the *d* spacing of Cloisite 15A is about 31 Å, quite large compared to that of Cloisite 30B, it is still considered that the PS/Cloisite 15A samples are intercalated despite of only about 2 Å extension of *d* spacing from Cloisite 15A.

3.2. Thermal stability

Thermal gravimetric analysis was conducted in nitrogen and results are shown in Fig. 3. Although previous studies did not conclusively exclude the effects of oxygen in surrounding air on thermal degradation of polymeric materials during burning of the polymers, oxidation reactions of the polymers appear to be insignificant (oxygen is mainly consumed by gas phase reactions – i.e., the flame). An exception is the case in which the flame does not cover the entire burning surface or the burning/pyrolysis rate is extremely low [20,21]. The addition of MWNTs to PS does not affect the thermal stability of PS. However, the addition of a small amount of Cloisite 15A (2% by mass) slightly increases the thermal stability of PS but further increase in the concentration of Cloisite 15A gradually reduces the increase in the thermal stability of PS. This could be due to the lower thermal stability of the organic treatment, dimethyl di-dehydrogenated tallow (starts to degrade at about 210 °C and loses about 35% of the original mass at 500 °C), on the clay surface of Cloisite 15A compared to thermal stability of PS. The addition of a small amount of SWNT to PMMA slightly reduces the thermal stability of PMMA below about 340 °C but slightly increases the thermal stability of PMMA above the temperature. The addition of Cloisite 30B slightly increases the thermal stability of PMMA (if the initial sample mass, W_0, is corrected by subtracting an amount of inorganic component of clay by assuming as an inert, the normalized sample mass curves shift toward lower temperature, which means less increase in thermal stability. This quantitative effect becomes larger with the amount of an inert in the sample). If the inorganic component of clay and the carbon nanotubes are assumed to be inert, then the amount of each residue is close to the amount of initial inert amount of each additive, these additives do not significantly enhance the amount of char (at most 2% with the clays). Overall, the addition of the four nanoparticles does not significantly affect the thermal stability of the two polymer matrixes, except possibly for PS/Cloisite 15A (2%).

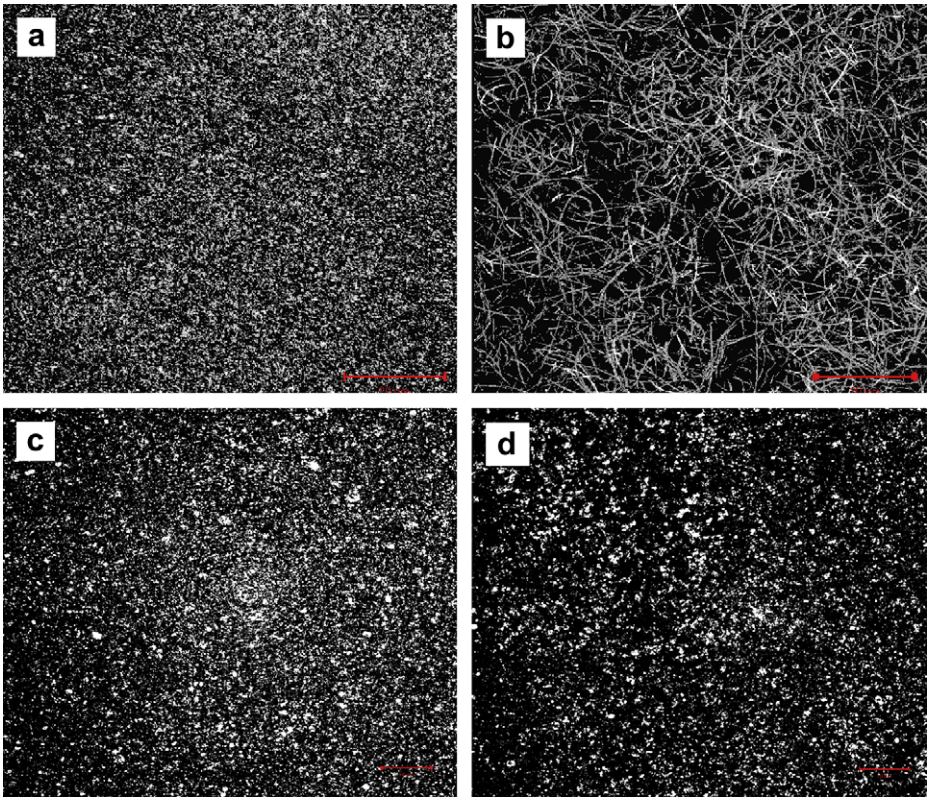

Fig. 1. Confocal microscopy images: (a) PMMA/SWNT (0.5%), (b) PS/MWNT (1%), (c) PMMA/Cloisite 30B (10%), and (d) PS/Cloisite 15A (10%). Each bar scale is 20 μm.

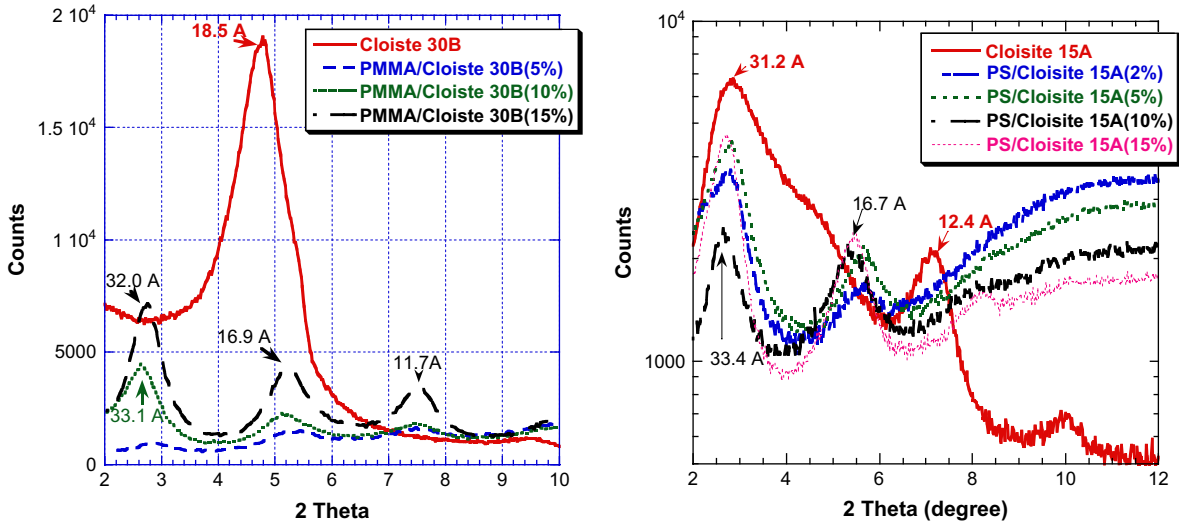

Fig. 2. XRD results of PMMA/Cloisite 30B samples and PS/Cloisite 15A samples.

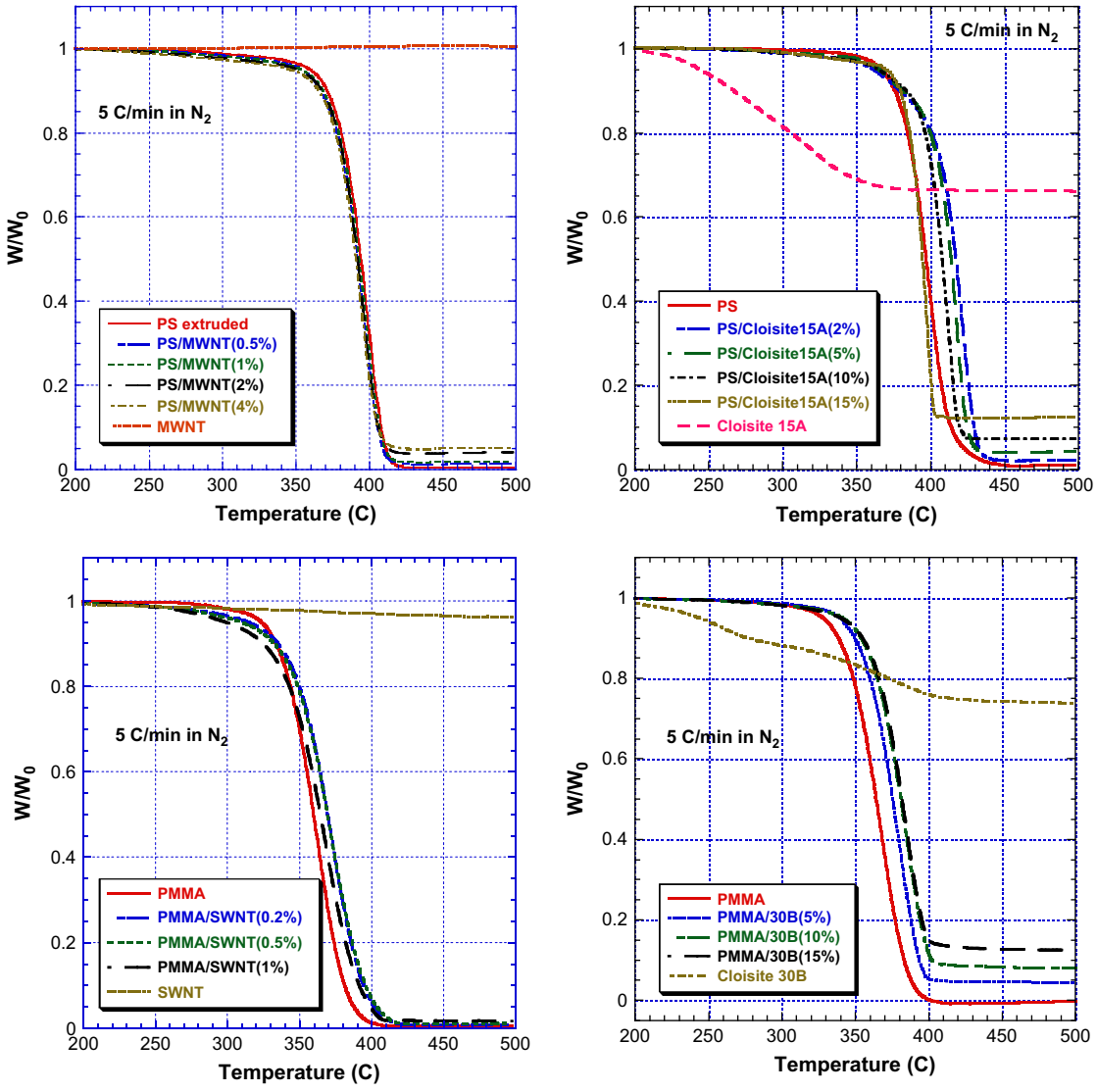

Fig. 3. TGA analysis of the PS/MWNT, PS/Cloisite 15A, PMMA/SWNT, and PMMA/Cloisite 30B at a heating rate of 5 °C/min in nitrogen.

3.3. Viscoelastic properties

The storage modulus G' provides a measure of nanocomposite "stiffness" and its frequency dependence characterizes whether the material is in a liquid-like or solid-like state [22]. The relations between G' and frequency are shown in Fig. 4 for the four nanocomposite samples. At 200 °C, PS/Cloisite 15A (2%) and PS/MWNT (0.5%) composites have nearly the same rheological response as pure PS showing the typical scaling behavior of $G' \sim \omega^2$ (where ω is the oscillatory frequency) at low frequencies. This trend is also observed for PMMA/SWNT (0.1%). Since the PMMA/Cloisite 30B samples were prepared by melt compounding using an extruder, the reduction in G' of the PMMA/Cloisite 30B and PMMA shown in Fig. 4 is due to a small reduction in molecular weight of PMMA during melt compounding, and similar reduction in G' has been observed for extruded polymer–clay nanocomposites at low clay concentrations [23,24]. Although the PS/MWNT samples were prepared by melt compounding at a low screw speed, the reduction in G' appears to be much smaller than in the case of the PMMA/Cloisite 30B samples. For the composites containing higher concentration of the clays and the carbon nanotubes (about 10% by mass for the both clays, about 2% for MWNT, and about 0.5% for SWNT), the above described liquid-like, low-frequency scaling of G' disappeared and G' becomes nearly constant at low frequencies. This indicates a transition from a liquid to an ideal Hookean solid, which accompanies the formation of a mechanically stable network structure [18,25,26].

The above viscoelastic measurements were conducted at 200 °C. However, the hottest regions of the samples would be in the temperature range of 350–400 °C during burning. Evidently, the persistence of the network structure becomes critical for effective flame retardancy at higher temperatures. The TGA results shown in Fig. 3 indicate that some of the composite samples start to degrade slowly at around 250 °C. For this reason, viscoelastic measurements were conducted from 160 °C to 240 °C at a frequency of 1 rad/s and the results are shown in Fig. 5. G' of PS/Cloisite 15A (10% and 15%) is nearly constant with temperature change even at 240 °C and much higher than G' of PS/MWNT composites (roughly one order higher than G' of PS/MWNT (2%)). G' of PMMA/Cloisite 30B (10% and 15%) is slightly decreasing with an increase in temperature but they are much higher than those of PMMA/SWNT composites. This trend indicates that the network structure in PS/Cloisite 15A and PMMA/Cloisite 30B at relatively high concentrations of the clays would be preserved at high temperatures, probably even during burning.

In our previous study [8], it was demonstrated that the formation of a network-structured protective layer consisting of carbon nanotubes during burning is necessary for the improvement in flammability properties of PMMA. If this applies to plate-shape nanoparticles such as clay, it is expected that PS/Cloisite 15A (10% and 15%) and PMMA/Cloisite 30B (10% and 15%) would form such a layer and their flammability properties would be significantly improved compared to those of PS and PMMA.

3.4. Flammability properties

The effects of the concentration of Cloisite 15A and MWNT on mass loss rate of PS are shown in Fig. 6. An increase in the level of Cloisite 15A significantly reduces the mass loss rate of PS up to 10% by mass. Above 10%, the reduction in mass loss rate is relatively small. This trend is also seen for PMMA/Cloisite 30B as shown in Fig. 7. An increase in the level of MWNT also significantly reduces the mass loss rate of PS, in particular, above 0.5% of mass. However, at the concentration of 4% by mass, mass loss rate becomes higher than that of PS/MWNT (2%) (not included in Fig. 6) due to an increase in the thermal conductivity of the composite. This trend was also observed with PP/MWNT composites [27] and PC/MWNT composites [28]. The mass loss rate results for PMMA/SWNT were obtained in our previous study [8] with 8 mm thick samples instead of 4 mm thick samples used in the present study. The effects of the sample thickness on mass loss rate at 50 kW/m^2 would be small when the sample thickness is relatively thick such as 4 mm. The addition of SWNT significantly reduces the mass loss rate of PMMA. Furthermore, the mass loss rate of PMMA/SWNT (1%) is slightly higher than that of PMMA/SWNT (0.5%), similar to the above case of PS/MWNT.

In Section 3.3, the measured viscoelastic characteristics indicate the effective formation of a network structure for some of the composite samples. If our hypothesis is correct, the residues of PS/Cloisite 15A (10% and 15%), PS/MWNT (2%), PMMA/Cloisite 30B (10% and 15%), and PMMA/SWNT (0.5% and 1%) collected after the gasification experiments should all form continuous protective layers without any significant openings such as cracks. The pictures of the collected residues after the gasification experiments are shown in Fig. 8 for PS series samples and in Fig. 9 for PMMA series samples. As expected, both pristine PS and pristine PMMA did not leave any significant amount of residue. At a low level of the nanoparticle loading in the polymer, the residues did not cover the

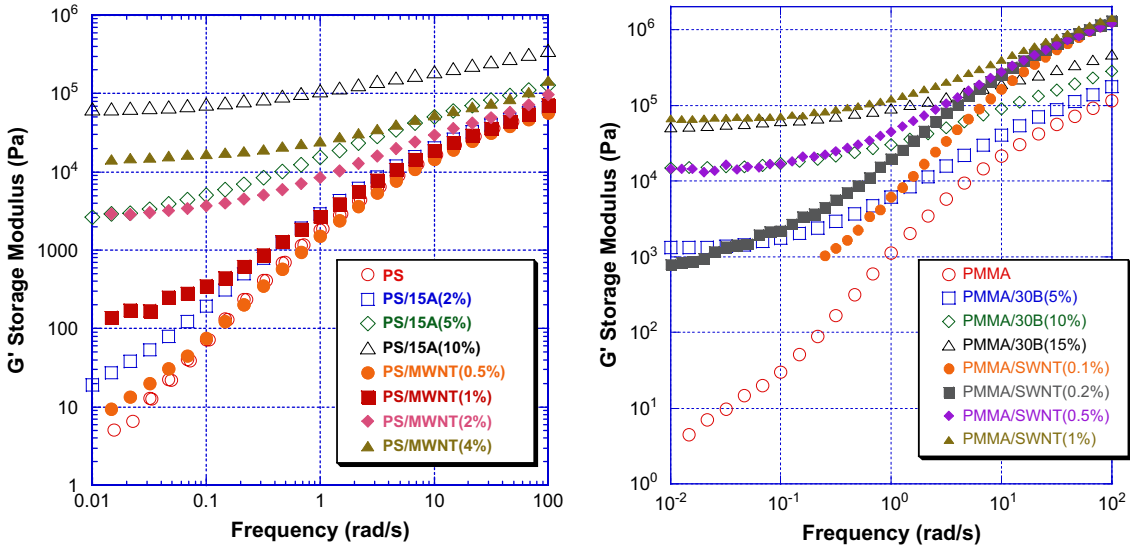

Fig. 4. Effects of the nanoparticle type and concentration on the relationship of storage modulus with respect to frequency measured at 200 °C.

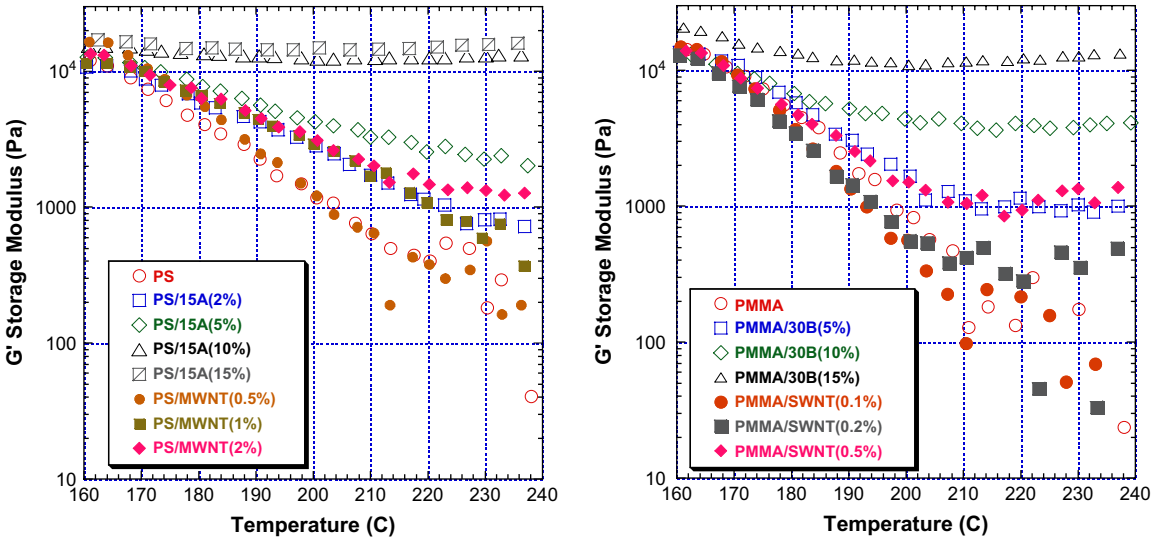

Fig. 5. Effects of the nanoparticle type and concentration on the relationship of storage modulus with respect to temperature measured at frequency rate of 1 rad/s.

sample container leaving a pattern consisted of many isolated clumps or islands. An increase in the level of either MWNT or SWNT led that the residues cover the entire sample container without any cracks or openings. However, the residues of PS/Cloisite 15A and PMMA/Cloisite 30B contain cracks and the size of the cracks became much smaller at 15% by mass of the clays. Since vigorous bubbling (evolving fuel to the gas phase) was observed through any opening or cracks, avoiding any such opening or crack is critical to reduce the mass loss rate (or heat release rate). If they were without any cracks, PS/Cloisite 15A (10% and 15%) and PMMA/Cloisite 30B (10% and 15%), the mass loss rates of the samples could be less than those shown in Figs. 6 and 7. The integrity of the nanoparticle network during burning is evidently crucial for effective flame retardancy; network formation is necessary but not sufficient condition for effective flammability reduction.

4. Discussion

Although the network structure is formed for PS/Cloisite 15A (10% and 15%) and PMMA/Cloisite 30B (10% and 15%) samples and the measured storage modulus G' is much higher than those of PS/MWNT and PMMA/SWNT at elevated temperatures, the images of the corresponding residues in Fig. 5 show many small cracks instead of continuous network-structure residues without any opening and cracks only for the latter samples. These cracks and openings should be avoided as much as possible to reduce mass loss rate because degradation products are evolved from the interior of the sample through cracks/opening by vigorous bubbling. If there are no cracks for the residues of clay-based samples, their mass loss rates would be less than those shown in Figs. 6 and 7. Therefore, it is important to understand why cracks are formed in the residues of the clay-based samples. Selected video images of the PS/Cloisite 15A (10%) during the radiant gasification experiment are shown in Fig. 10. At 20 s from the start of the exposure to the external radiation, extremely fine bubbles cover the entire sample surface. At 41 s, the color of the sample surface starts to get darker and at 49 s the sample surface becomes a quite dark color, except near the perimeter of the sample. A small sample mass loss starts at about 40 s. At 58 s, the dark color starts to fade with appearance of many cracks. At 70 s, cracks are

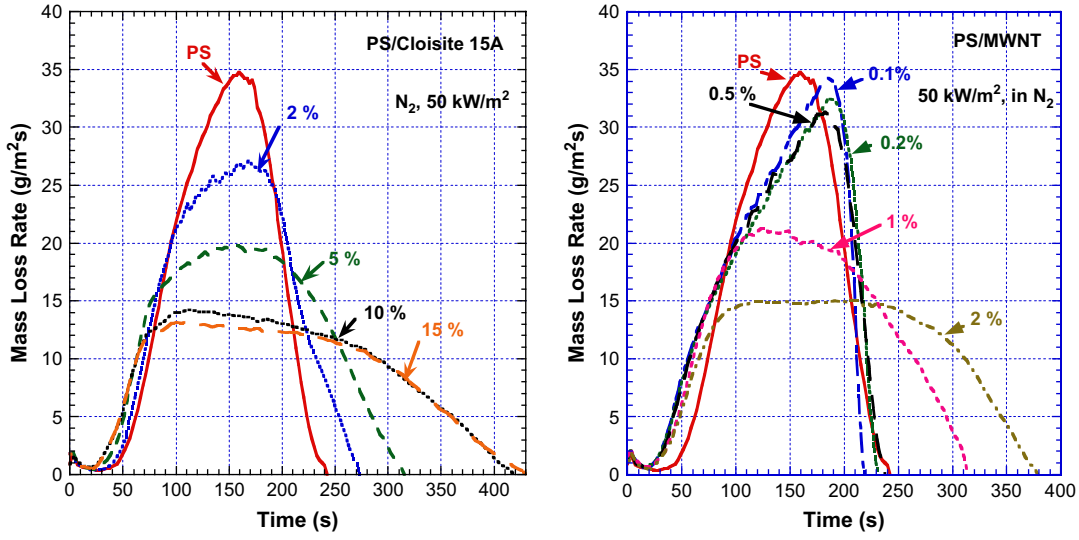

Fig. 6. Effects of concentration of Cloisite 15A and MWNT on mass loss rate of PS at an external radiant flux of 50 kW/m^2 in a nitrogen atmosphere.

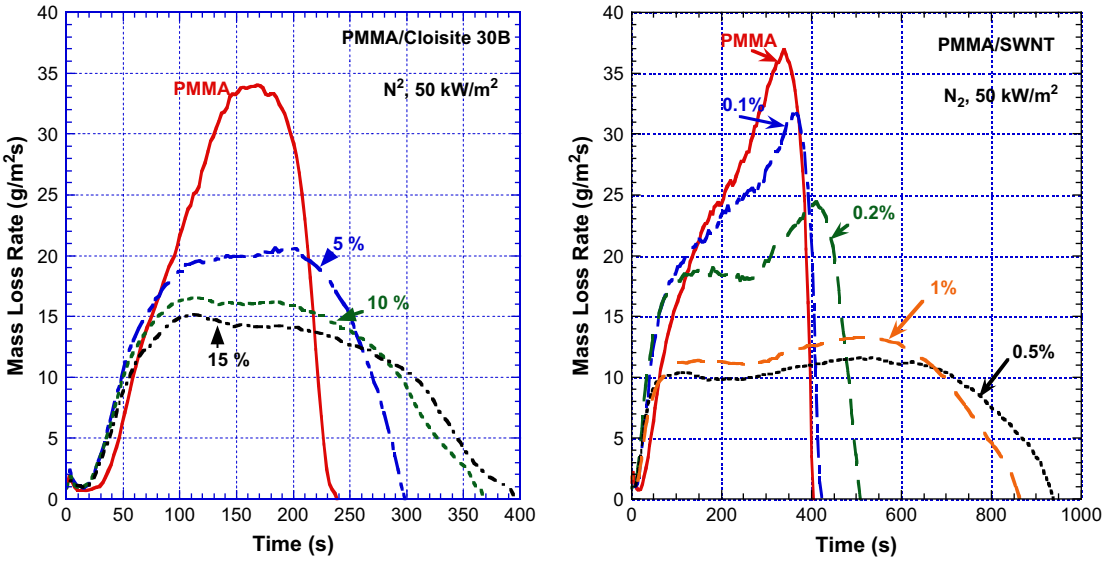

Fig. 7. Effects of concentration of Cloisite 30B and SWNT on mass loss rate of PMMA at an external radiant flux of 50 kW/m^2 in a nitrogen atmosphere.

established and they get deeper/wider as shown at 110 s. These images show that cracks are formed at relatively early time and they became deeper and wider and remain at the same locations until the end of the test. The cracks go through the residue and they could be the major path for the evolved degradation products to the gas phase. These video images clearly show that the cracks form nearly at the start of mass loss for the sample when the layer containing the cracks is relatively thin and limited to near the sample surface.

The formation of a network structure occurs more readily with higher aspect ratio nanoparticles and with a rod-like particle compared to a plate-like particle [25,29,30]. The average aspect ratio of the SWNT in PMMA was about 45 [18] and that of the MWNT in PS was about 150 [19]. From the SEM images described below, the average aspect ratio of the clay particles was about 200. Thus, while the aspect ratio of the clays tends to be slightly larger than those of the carbon nanotubes, the network had less integrity at high temperature burning conditions. It is not clear how the integrity of network formation as determined in relatively low temperature (below 250 °C) rheological measurements can be used to predict network stability under burning conditions (~400 °C). Again, network formation at relatively low temperatures is a necessary condition, but it may be insufficient to predict network integrity at high temperatures.

In order to understand the structure of the residues, SEM images of the four residues of PS/Cloisite 15A (10%), PS/MWNT (2%), PMMA/Cloisite 30B (10%), and PMMA/SWNT (0.5%) were taken and are shown in Fig. 11. Aggregates of numerous clay platelets are shown in the residue of PS/Cloisite 15A (10%) compared to entangled MWNTs in the residue of PS/MWNT (2%). The magnified images (scale bar of 200 nm) show clay platelets with voids among the platelets as seen in the residue of

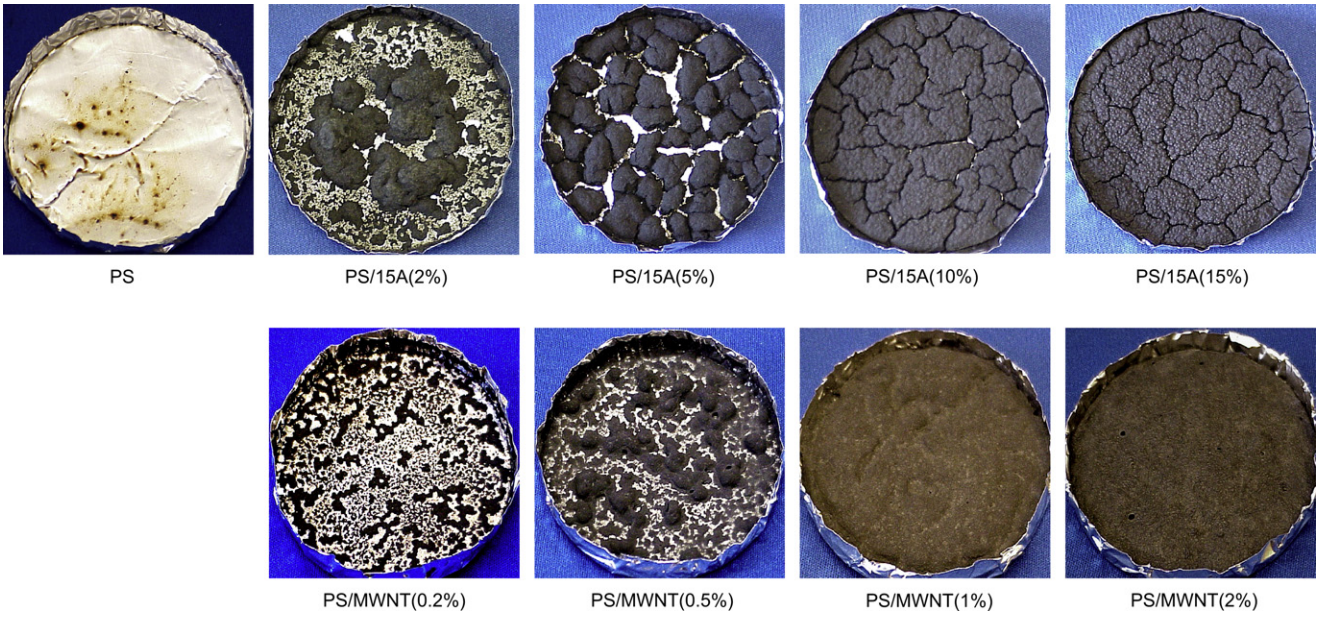

Fig. 8. Pictures of the residues of PS/Cloisite 15A and PS/MWNT collected after the gasification tests.

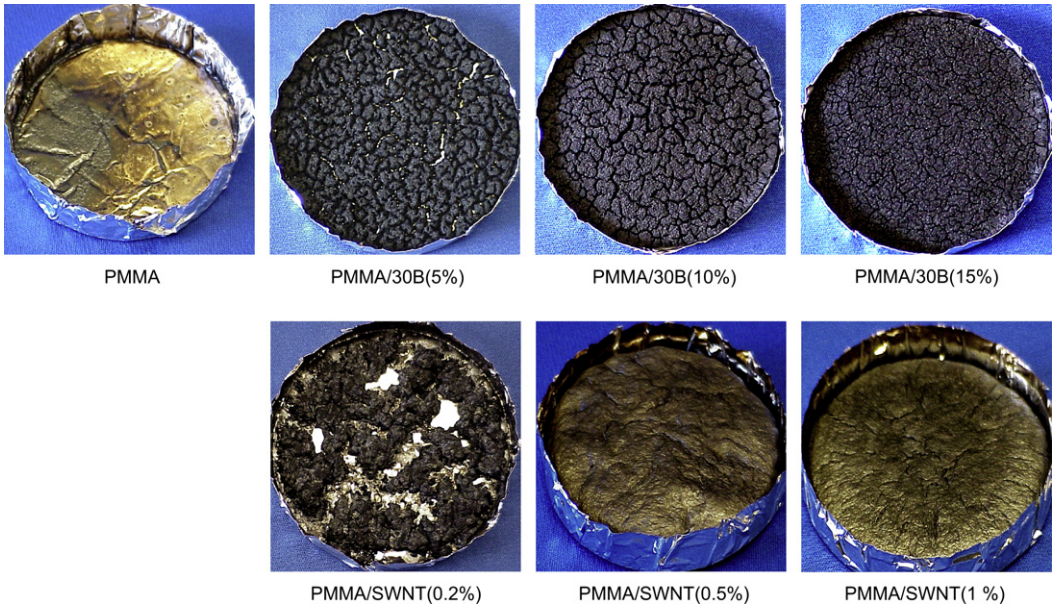

Fig. 9. Pictures of the residues of PMMA/Cloisite 30B and PMMA/SWNT collected after the gasification tests.

PMMA/Cloisite 30B (10%). In contrast, extremely entangled and dense network structures involving numerous tubes are seen in the residue of PMMA/SWNT (0.5%). A qualitative difference between clay particles and carbon nanotubes in these residues appears to be a much higher degree of entanglement and bridging of the tubes (multiple contact with other tubes) compared to that of clay platelets. Also, it appears that there are more voids (open spaces between clay platelets) compared to the case with carbon nanotubes in the residues so that the entanglement density of clay platelets tends to be less than that with carbon nanotubes. When a composite sample starts to loose some mass, a thin layer consisting of the clay platelets or the carbon nanotubes is formed after the polymer resin degrades and its degradation products evolve to the gas phase. The temperature distribution near the sample surface is steep at early times. Since the thermal conductivity of carbon nanotubes is quite high [31,32], the layer consisting of the tubes might have a more nearly uniform temperature compared to a possible steep temperature gradient through the layer consisting of clay platelets. Furthermore, the tubes tend to be highly entangled and bridging so that the physical strength of the layer would be strong enough to remain intact against numerous minute bubbles evolving from the interior of the sample. Although the residue is soft and can be squeezed by hand without fracturing, no swelling is observed during the radiative gasification test. This

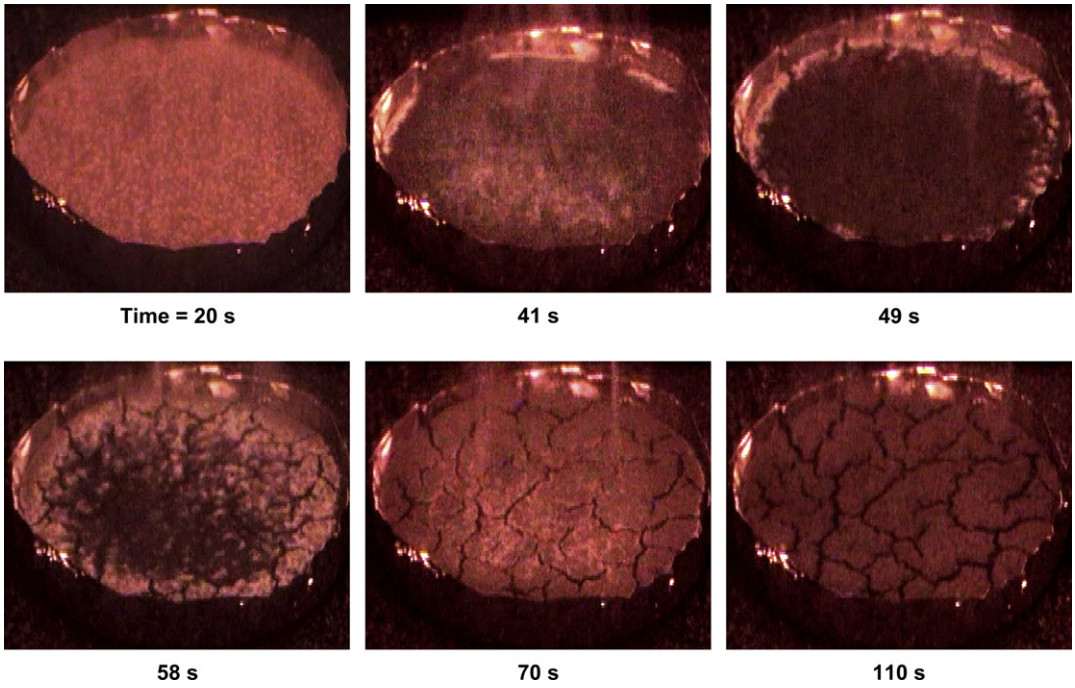

Fig. 10. Sample behavior of PS/Cloisite 15A (10%) in nitrogen after an exposure to external radiant flux of 50 kW/m^2.

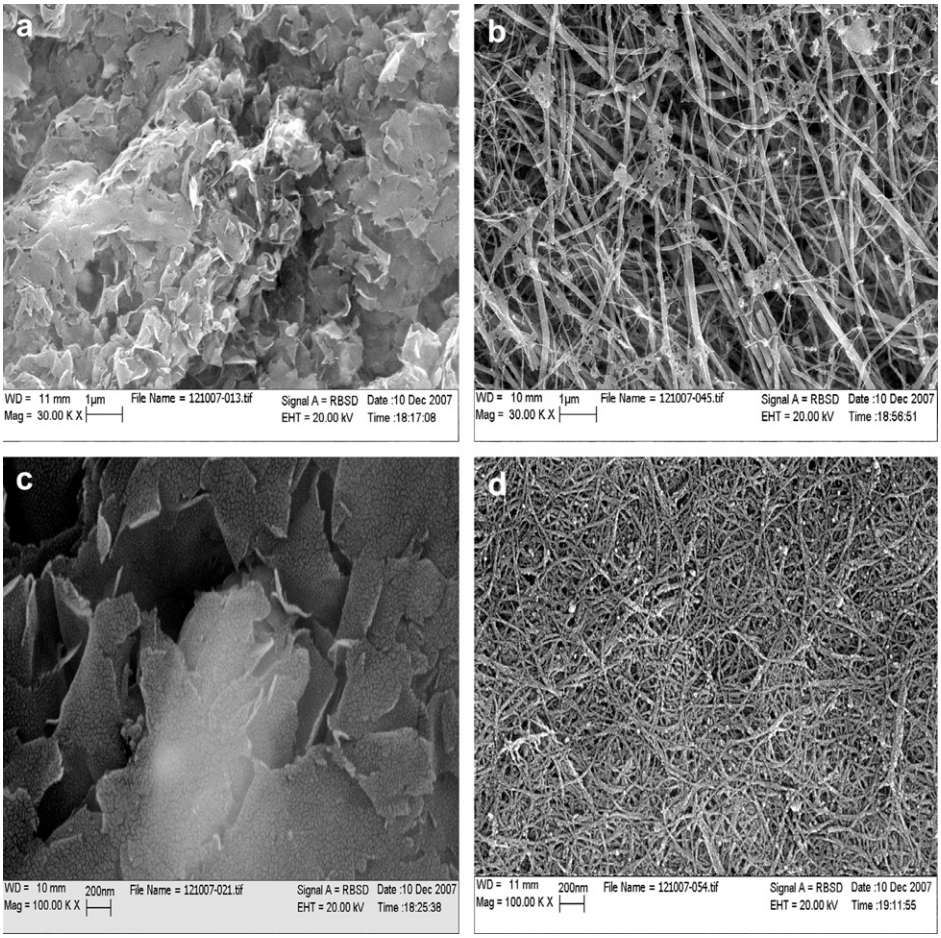

Fig. 11. SEM images of the residues collected after the gasification tests: (a) PS/Cloisite 15A (10%), scale bar of 1 μm; (b) PS/MWNT (2%), scale bar of 1 μm; (c) PMMA/Cloisite 30B (10%), scale bar of 200 nm, and (d) PMMA/SWNT (0.5%), scale bar of 200 nm.

indicates that degradation products evolve through the dense entangled tube layer, possibly with capillary motion of the liquefying polymer resin, without interior pressure building. On the other hand, the layer consisting of clay platelets tends to have voids and there is less entangling of platelets so that bubbles evolving from the interior of the sample enlarge the existing openings and push away the platelets to form larger openings throughout the layer. These openings merge and finally form cracks.

The openings could be formed from thermal degradation of organic treatments on the clay platelets. The TGA data of Cloisite 15A show about 34% mass loss at 500 °C in nitrogen and Cloisite 30B loses about 26% of mass. The expanding, evolved degradation products from the clay platelets could further enlarge the distance between platelets. However, the average distance between clay platelets in the residues of PMMA/Cloisite 30B measured by XRD is about 12.5 Å (as shown in Fig. 13) and that of the residues of PS/Cloisite 15A is about the same (data not shown) which is less than the platelet distance of both initial nanocomposite samples (32–33 Å for PMMA/Cloisite 30B and 31–33 Å for PS/Cloisite 15A as shown in Fig. 2). Therefore, the loss of the organic treatment on clay platelets does not contribute to the above described opening. Furthermore, the TGA results of the SWNT and the MWNT show that the former loses about 10% of its mass and the latter loses about 1% of its mass at 500 °C in nitrogen under heating rate of 5 °C/min. It appears that these mass loses do not significantly modify the network of the carbon nanotubes.

Another possible process to consider is breaking of the thin, hard and brittle clay–platelets layer under heat stress created by the steep temperature gradient in the beginning of the test. It is theoretically predicted that there are more entangling and bridging among rod-shaped nanoparticles than sheet-shape nanoparticles [30]. Evidently, having a gel network is not enough to universally impart flammability reduction, the network must be stable under burning conditions.

The trend of less effective flame retardancy for clay-based nanocomposites as compared to carbon nanotube-based nanocomposites at the same nanoparticle mass concentration can be seen by comparing the relationship between the normalized storage modulus measured at a low frequency and the normalized mass loss rate of the two nanocomposites, as shown in Fig. 12. The lower the normalized peak mass loss rate the better the fire performance. The figure shows clearly that PS/MWNT has a lower peak mass loss rate compared with PS/Cloisite 15A at the same value of the normalized storage modulus except for the samples that do not form a network structure. The concept of the formation of the network-structured protective layer with nanoparticles to improve flammability of polymers applies not only to carbon nanotubes but also to clay platelets. However, the tubes with their large aspect ratio, dense entanglement network and strong bridging interaction form physically stronger network compared to the less entangled clay platelets. Evidently, the network formed from clay-based nanocomposites does not appear to be strong enough to resist bubbles that push through voids among the platelet clusters and create cracks compromising the protection

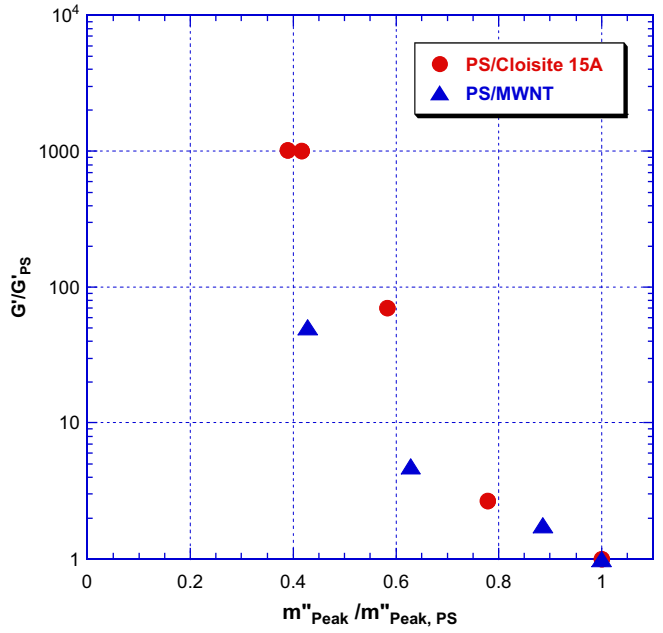

Fig. 12. Comparison of flame retardant efficiency between PS/Cloisite 15A and PS/MWNT. G' is measured at 200 °C and a frequency of 0.1 rad/s. m''_{peak} is the obtained peak mass loss rate of samples from Fig. 6 and normalized by the peak mass loss rate of PS.

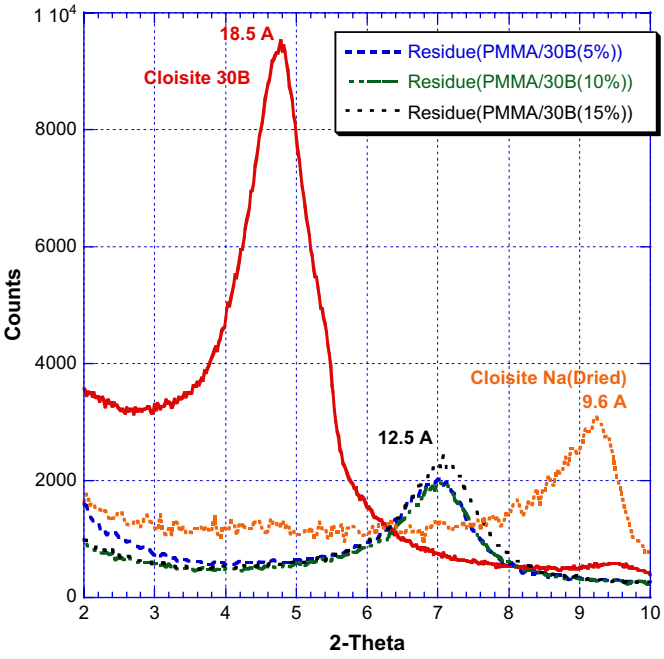

Fig. 13. XRD results of the residues of PMMA/Cloisite 30B collected after the gasification tests at 50 kW/m^2 in nitrogen.

layer. Correspondingly, this explains why the flammability properties of the clay-based polymer nanocomposites are not as good as those of carbon nanotube-based nanocomposites at relatively low particle concentrations.

5. Conclusion

The viscoelastic characteristics of PS/Cloisite 15A and PMMA/Cloisite 30B nanocomposites show the formation of a network structure in the range of 10–15% by mass compared to about 2% for PS/MWNT and 0.5% for PMMA/SWNT nanocomposites. The concept of the requirement of the formation of the network structure to achieve a significant improvement in flammability of polymer nanocomposites applies to the use of both clay and carbon nanotubes as a filler. Thus, while viscoelastic characterization of polymer nanocomposites can be used as a screening method for seeking effectively flame retarded nanocomposites, the formation and stability of the network structure also require good spatial dispersion of the clay platelets and carbon nanotubes in the nanocomposites. During burning, the effective flame retarded nanocomposites must exhibit a residue that covers the entire sample surface without any openings so as to suppress vigorous bubbling that would otherwise rapidly transports degradation products from the interior of the sample to the gas phase. This suppression of bubble transport process is observed with PS/MWNT and PMMA/SWNT having the network structure. However, PS/Cloisite 15A and PMMA/Cloisite 30B with the network produce the residues with many cracks (allowing vigorous bubbling through the cracks). These cracks are formed at a relatively early period of the test. The SEM images of the residues show densely entangled carbon nanotubes compared to less entangled clay platelets with voids. It is proposed that the physical integrity of the densely entangled carbon nanotubes layer is strong enough to remain intact during burning, while the less entangled clay platelets are disrupted by bubbles evolving from the interior of the sample. If polymer–clay nanocomposites could be made to form more stable network without forming any cracks during burning (one possible approach might be reinforcing the network with char using char forming resins), the flammability properties of the clay-based polymer nanocomposites could be further improved.

Acknowledgement

The authors would like to thank Dr. Thomas Ohlemiller at NIST for valuable discussion on flammability mechanisms of the nanocomposites. T.K. gratefully acknowledges funding from the FAA Technical Center under Grant 02-G-022.

References

[1] Gilman JW, Jackson CL, Morgan AB, Harris Jr R, Manias E, Giannelis EP, et al. Chem Mater 2000;12:1866–73.
[2] Kashiwagi T, Grulke EA, Hilding J, Harris Jr RH, Awad WH, Douglas J. Macromol Rapid Commun 2002;23:761–5.
[3] Bourbigot S, Vanderhart DL, Gilman JW, Bellayer S, Stretz H, Paul DR. Polymer 2004;45:7627–38.
[4] Morgan AB. Polym Adv Technol 2006;17:206–17.
[5] Morgan AB, Wilkie CA, editors. Flame retardant polymer nanocomposites. Hoboken, N.J: Wiley Inter-Science; 2007.
[6] Kashiwagi T. Proc Combust Inst 1994;28:1423–37.
[7] Clift R, Grace JR, Weber ME. Bubbles, drops, and particles. New York: Academic Press; 1978.
[8] Kashiwagi T, Du F, Douglas JF, Winey KI, Harris RH, Shields JR. Nat Mater 2005;4:928–33.
[9] Bartholmai M, Schartel B. Polym Adv Technol 2004;15:355–64.
[10] Ma H, Tong L, Xu Z, Fang Z. Polym Degrad Stab 2007;92:1439–45.
[11] Ren J, Silva AS, Krishnamootri R. Macromolecules 2000;33:3739–46.
[12] Wagener R, Reisinger JG. Polymer 2003;44:7513–8.
[13] Kashiwagi T, Fagan J, Douglas JF, Yamamoto K, Heckert AN, Leigh SD, et al. Polymer 2007;48:4855–66.
[14] Krishnamoorti R. MRS Bull 2007;32:341–7.
[15] Andrews R, Jacques D, Rao AM, Derbyshire F, Qian D, Fan X, et al. Chem Phys Lett 1999;303:467–74.
[16] Du F, Fischer JE, Winey KI. J Polym Sci Part B Polym Phys 2003;41:3333–8.
[17] Austin PJ, Buch RR, Kashiwagi T. Fire Mater 1998;22:221–37.
[18] Du F, Scogna RC, Zhou W, Brand S, Fischer JE, Winey KI. Macromolecules 2004;37:9048–55.
[19] Cipiriano BH, Kashiwagi T, Raghavan SR, Yang Y, Grulke EA, Yamamoto K, et al. Polymer 2007;48:6086–96.
[20] Brauman SK. J Polym Sci Chem Ed 1975;26:1159–71.
[21] Kashiwagi T, Ohlemiller TJ. Proc Combust Inst 1982;19:815–23.
[22] Kharchenko SB, Douglas JF, Obrzut J, Grulke EA, Milger KB. Nat Mater 2004;3:564–8.

[23] Wang K, Lian S, Deng J, Yang H, Zhang Q, Fu Q, et al. Polymer 2006;47:7131–44.
[24] Treece MA, Oberhauser JP. Polymer 2007;48:1083–95.
[25] Bicerano J, Douglas JF, Brune DA. JMS Rev Macromol Chem Phys 1999;C39:561–642.
[26] Hobbie EK, Fry DJ. J Chem Phys 2007;126:124907.
[27] Kashiwagi T, Grulke E, Hilding J, Groth K, Harris R, Butler K, et al. Polymer 2004;45:4227–39.
[28] Schartel B, Braun U, Knoll U, Bartholmai M, Goering H, Neubert D, et al. Polym Eng Sci 2008:149–58.
[29] Celard A, McRae E, Deleuze C, Dufort M, Furdin G, Mareche JF. Phys Rev B 1996;53:6209–14.
[30] Knauert ST, Douglas JF, Starr FW. J Polym Sci Part B Polym Phys 2007;45:1882–97.
[31] Kim P, Shi L, Majumdar A, McEuen PL. Phys Rev Lett 2001;87:215502.
[32] Yi W, Lu L, Zhang DL, Pan ZW, Xie SS. Phys Rev B 1999;59:R9015–8.